The Astrophysical Journal, 695:L125–L129, 2009 April 20 doi:10.1088/0004-637X/695/2/L125

STRUCTURE AND HISTORY OF DARK MATTER HALOS PROBED WITH GRAVITATIONAL LENSING

A. Lapi[1,2] and A. Cavaliere[1,3]
[1] Astrofisica, Dip. Fisica, Univ. "Tor Vergata," via Ricerca Scientifica 1, 00133 Roma, Italy
[2] Astrophysics Sector, SISSA/ISAS, Via Beirut 2-4, 34014 Trieste, Italy
[3] Accademia dei Lincei, Via Lungara 10, 00165 Roma, Italy
Received 2008 December 11; accepted 2009 March 9; published 2009 March 27

ABSTRACT

We test with gravitational lensing (GL) data the dark matter (DM) halos embedding the luminous baryonic component of galaxy clusters; our benchmark is provided by their two-stage cosmogonical development that we compute with its variance, and by the related "α-profiles" we derive. The latter solve the Jeans equation for the self-gravitating, anisotropic DM equilibria, and yield the radial runs of the density $\rho(r)$ and the velocity dispersion $\sigma_r^2(r)$ in terms of the DM "entropy" $K \equiv \sigma_r^2/\rho^{2/3} \propto r^\alpha$ highlighted by recent *N*-body simulations; the former constrains the slope to the narrow range $\alpha \approx 1.25$–1.3. These physically based α-profiles meet the overall requirements from GL observations, being intrinsically flatter at the center and steeper in the outskirts relative to the empirical Navarro, Frenk, & White formula. Specifically, we project them along the line of sight and compare with a recent extensive data set from strong and weak lensing observations in and around the cluster A1689. We find an optimal fit at both small and large scales in terms of a halo constituted by an early body with $\alpha \approx 1.25$ and by recent extensive outskirts, that make up an overall mass $10^{15}\ M_\odot$ with a concentration parameter $c \approx 10$ consistent with the variance we compute in the ΛCDM cosmogony. The resulting structure corresponds to a potential well shallow in the outskirts as that inferred from the X rays radiated from the hot electrons and baryons constituting the intracluster plasma.

Key words: dark matter – galaxies: clusters: general – galaxies: halos – gravitational lensing – X-rays: galaxies: clusters

1. INTRODUCTION

The collisionless, cold dark matter (CDM) particles that constitute the gravitationally dominant component of galaxy clusters are distributed in a "halo" embedding the electromagnetically active baryons. The halo development under self-gravity from small density perturbations has been focused by several recent *N*-body simulations, with three main outcomes.

First, the growth is recognized (Zhao et al. 2003; Hoffman et al. 2007; Diemand et al. 2007) to comprise two cosmogonic stages: an early fast collapse including a few violent major mergers and building up the halo "body"; a later, quasi-equilibrium stage where the outskirts develop from the inside-out by minor mergers and smooth accretion (see Salvador-Solé et al. 2007). The *transition* occurs at the redshift z_t when a DM gravitational well attains its maximal depth, or the radial peak of the circular velocity $v_c^2 \equiv GM/R$ its maximal height (see Li et al. 2007). This sharp definition of halo "formation" also marks the time for the early gravitational turmoil to subside.

Second, the ensuing quasi-equilibrium structure is effectively expressed in terms of the functional $K \equiv \sigma_r^2/\rho^{2/3}$ that combines the density ρ and the radial velocity dispersion σ_r^2 in the form of a DM "entropy" (or rather "adiabat"; see Bertschinger 1985; Taylor & Navarro 2001; Hoffman et al. 2007; Vass et al. 2008). This mimics the behavior of a thermodynamic entropy in that it increases in the halo bodies during the fast collapses and stays put during the subsequent quiet accretion.

Third, the simple run $K(r) \propto r^\alpha$ is empirically found to hold in the settled halo bodies, with slopes around 1.25 (see Navarro et al. 2008). This apparently universal halo feature allows recasting the pressure $\rho(r)\,\sigma_r^2(r) \propto K(r)\,\rho^{5/3}(r)$ in terms of density, to balance self-gravity for the equilibrium.

As to the latter we have used the isotropic Jeans equation to derive the "*α-profiles*" for DM quantities such as $\rho(r)$ and $\sigma_r^2(r)$, having ascertained that α lies within the narrow range 1.25–1.3 from a state-of-the-art semianalytical study of the cosmogonic halo development; see Lapi & Cavaliere (2009, hereafter LC09).

In this Letter, we first refine these profiles to conditions of developing outskirts and anisotropic velocity dispersion; then we test them against recent data that join observations of strong and weak gravitational lensing (GL).

2. HALO DEVELOPMENT AND EQUILIBRIUM

Our framework will be provided by the standard Λ-cosmology, i.e., a flat universe with normalized matter density $\Omega_M = 0.27$, dark energy density $\Omega_\Lambda = 0.73$, and Hubble constant $H_0 = 72$ km s^{-1} Mpc^{-1}. To bridge the matter- to the dark energy-dominated era across the cosmological crossover at $z \approx 0.5$, we shall express the redshift–time relation $(1+z) \propto t^{-q}$ in terms of the parameter q growing from 2/3 to 4/5.

2.1. The Entropy Slope From Cosmogonic Development

The evolutions of the current bounding radius R, of the circular velocity v_c^2, and of the entropy K are obtained by LC09 in terms of the halo mass M and its growth rate $\dot{M}$ from the simple scaling laws $R \propto M/\dot{M}^{2/3}$, $v_c^2 \propto \dot{M}^{2/3}$, and $K \propto R\,M^{1/3}$. Whence straightforward algebra leads to express the entropy slope $\alpha \equiv d\log K/d\log R$ as

$$\alpha = 1 + \frac{1}{1 + 2\,\epsilon/q}, \tag{1}$$

in terms of the inverse growth rate $\epsilon \equiv -d\log(1+z)/d\log M = q\,M/\dot{M}\,t$.

With $\epsilon \approx 1$ marking the cosmogonic transition from fast to slow accretion as gauged on the running Hubble timescale, it is seen from Equation (1) that the range $\alpha \approx 1.25$–1.3 will apply to average halos that began their slow accretion in the corresponding interval $z_t \approx 1.5$–0.2. The range of α is narrow

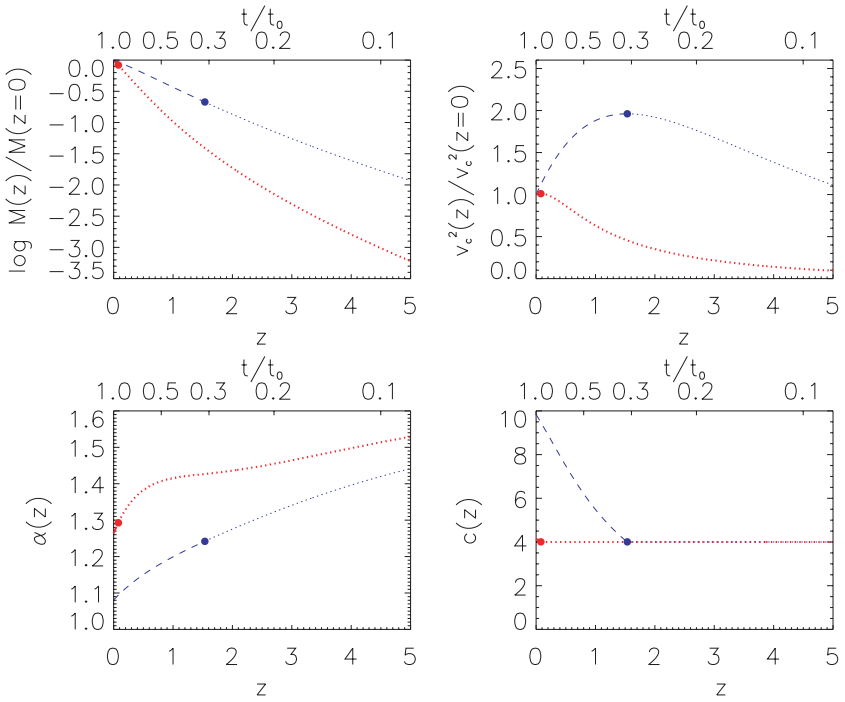

Figure 1. Evolutionary track of a halo's mass M, circular velocity v_c^2, entropy slope α, and concentration c for a current overall mass of $10^{15}\,M_\odot$. In all panels, red lines refer to the history of an *average* cluster, while blue ones refer to the main progenitor to illustrate the *variance* (see Section 2.1 for details). Lines are dotted during the fast collapse of the halo body, and dashed during the slow accretion of the outskirts; big dots locate the cosmogonic *transition*, when $\alpha = 1.29$ and 1.25 are seen to hold (bottom left panel) for the average and the main progenitor history, respectively. During the subsequent slow accretion, such values are retained in the halo body, while they slowly decrease at the outskirts' boundary following $\alpha(z)$.

as the evolution of $\epsilon(t)/q(t)$ is *slower* than for $\epsilon(t)$ and $q(t)$ separately, which explains why closely similar values of α are found in halo bodies from different simulations.

Such a behavior is checked and refined in terms of the detailed evolution of $\epsilon(t)$; its *average* evolutionary track is obtained from integrating for $M(t)$ the differential equation

$$\dot{M}(M,t) = \int_0^M dM'(M - M')\,\frac{d^2\,P_{M'\to M}}{d\,M'd\,t}, \qquad (2)$$

with the state-of-the-art *kernel* detailed in Appendix A of LC09. We illustrate as red lines in Figure 1 our outcomes for an average cluster with current overall mass $M \approx 10^{15}\,M_\odot$; we plot the redshift evolution of the mass $M(z)$, the circular velocity $v_c(z)$, and the entropy slope $\alpha(z)$. Note that our approach, which includes ellipsoidal collapse of the body and outskirts growth controlled by Λ, renders the peaked behavior of $v_c^2(t)$ in remarkable agreement with the detailed simulations. For $M \approx 10^{15}\,M_\odot$, the transition occurs at $z_t \approx 0.2$, the entropy slope at z_t is around $\alpha \approx 1.3$, and the outskirts are currently rudimentary.

But considerable *variance* arises from the stochastic nature of the individual growth histories. As an example of variant, early *biased* track we focus on the one associated with the "main progenitor" that constitutes the main branch of a merging tree (illustrated, e.g., in Cavaliere & Menci 2007, their Figure 1). Such a history is obtained from the same Equation (2), with the lower integration limit replaced by $M/2$; the results for a *current* mass $M \approx 10^{15}\,M_\odot$ are shown as blue lines in Figure 1. Relative to the average, this history features a higher transition redshift $z_t \approx 1.5$, a less massive body with $M \approx 2 \times 10^{14}\ M_\odot$, an entropy slope $\alpha \approx 1.25$, and currently extensive outskirts. We find the occurrence of such biased halos relative to the average to be 0.125:1 on integrating the kernel of Equation (2) over the corresponding two histories.

An imprint of the transition redshift z_t is provided by the concentration parameter $c(z)$, that scales in overall terms as $[M(z)/M(z_t)]^{1/3}$; in fact, Zhao et al. (2003) and Wechsler et al. (2006) describe its increase for $z < z_t$ with the approximation $c(z) \approx 4\,(1 + z_t)/(1 + z)$, adopted in the bottom right panel of our Figure 1. It is seen that for the average history the present concentration reads $c \approx 4$, while for the main progenitor it takes on values $c \approx 10$.

From overall halo development we now turn to profiles for the equilibrium following the transition time.

2.2. α-Profiles From Jeans Equilibrium

Physical profiles are derived from the above values of α inserted into the radial Jeans equation, with pressure $\rho\sigma_r^2 \propto r^\alpha\,\rho^{5/3}$ and anisotropy described in terms of the standard Binney (1978) parameter $\beta \equiv 1 - \sigma_\theta^2/\sigma_r^2$. In terms of the density slope $\gamma \equiv -d\log\rho/d\log r$, Jeans may be recast to read

$$\gamma = \frac{3}{5}\left(\alpha + \frac{v_c^2}{\sigma_r^2}\right) + \frac{6}{5}\,\beta. \qquad (3)$$

When supplemented with the mass definition $M(<r) \equiv 4\pi\int_0^r dr' r'^2\,\rho(r')$ entering v_c^2, this constitutes an integrodifferential equation for $\rho(r)$, that by double differentiation reduces to a handy second-order differential equation for γ (Austin et al. 2005; Dehnen & McLaughlin 2005).

With $\alpha = \text{const}$ and $\beta = 0$ (meaning isotropy), LC09 found that physical solutions, which we named "α-profiles," exist for $\alpha \leqslant 35/27 = 1.\overline{296}$. The corresponding density runs steepen monotonically outward and satisfy physical central and outer boundary conditions, respectively: a round minimum of the

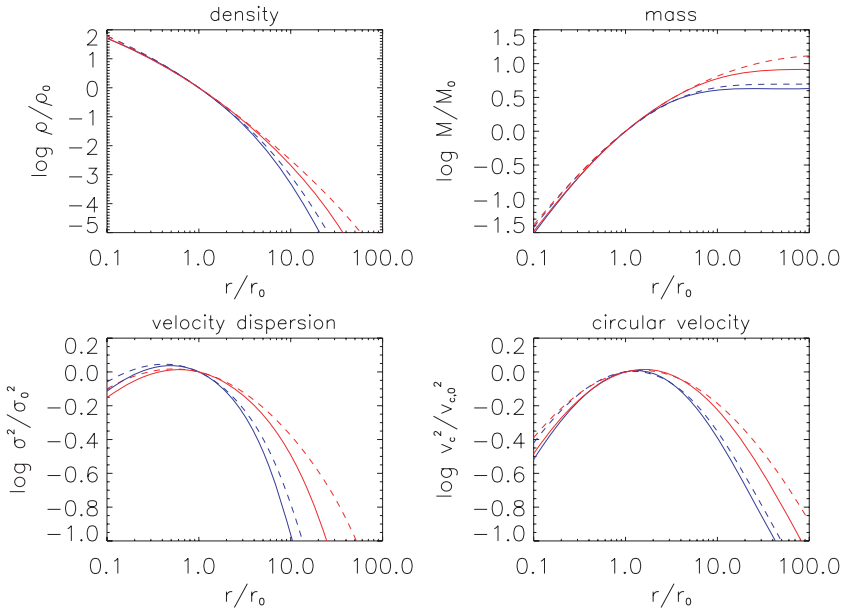

Figure 2. Radial runs for the α-profiles: density ρ, mass M, velocity dispersion σ_r, and circular velocity v_c; the profiles are normalized to 1 at the point r_0 where $\gamma = \gamma_0$ holds (see Equation (4)), with the main body spanning the range $r \lesssim 2\,r_0$. Curves are for $\alpha = 1.25$ (blue) and 1.29 (red), in the isotropic (dashed) and anisotropic (solid) equilibria; we adopt the anisotropy given in Equation (5) with $\beta(0) = -0.1$ and $\beta' = 0.2$, the latter parameter being actually irrelevant (see Section 3.1).

potential along with a round maximum of the pressure; a finite (hence definite) overall mass. In Figure 2, we report as dashed lines the *α-profiles* for various quantities: density $\rho(r)$, mass $M(< r)$, circular velocity $v_c^2(r)$, and velocity dispersion $\sigma_r^2(r)$.

The behavior of the density run (the top left panel of Figure 2) is highlighted by the analytical expressions of the slopes

$$\gamma_a \equiv \tfrac{3}{5}\,\alpha, \quad \gamma_0 \equiv 6 - 3\alpha, \quad \gamma_b \equiv \tfrac{3}{2}\,(1+\alpha). \tag{4}$$

These start with the central ($r \to 0$) value $\gamma_a \approx 0.75$–078, progressively steepen to $\gamma_0 \approx 2.25$–2.1 at the point r_0 that marks the halo main body, and steepen further into the outskirts to the value $\gamma_b \approx 3.38$–3.44.

Monotonic behavior and physical boundary conditions for the α-profiles are seen (e.g., LC09) to imply a maximal value $\kappa_{\rm crit}(\alpha) = v_c^2/\sigma^2 \approx 2.6$–$2.5$ in the body, at the point $r_p \gtrsim r_0$ where $v_c^2(r)$ peaks (see Figure 2, bottom right panel); there the slope reads $\gamma_p = 3\,(\alpha + k_{\rm crit})/5 \approx 2.32$–$2.28$ after Equation (3).

Thus, the inner slopes are considerably *flatter* as to yield a smooth central pressure, while the outer one is *steeper* as to yield a definite overall mass, compared to the empirical Navarro, Frenk, & White formula (NFW; Navarro et al. 1997). The latter, in fact, implies infinite mass, and angled central pressure and potential.

The concentration parameter for the α-profiles is given in detail by $c \equiv R/r_{-2}$ in terms of the radius r_{-2} where $\gamma = 2$. This may be viewed as a measure of central condensation (small r_{-2}) and/or outskirts' extension (large R).

3. CLUSTER PROFILES TESTED WITH GL OBSERVATIONS

A significant observational test requires to go *beyond* the limitations to $\alpha =$ const and isotropy; we tackle these issues in turn.

3.1. Refined α-Profiles

As to the latter, here we include on the right-hand side of Equation (3) the anisotropy term. This clearly will *steepen* the density run for positive β meaning radial dominance, as expected in the outskirts from infalling cold matter. Tangential components must develop toward the center, as expected from increasing importance of angular momentum effects (see LC09), and as supported by numerical simulations (Austin et al. 2005; Hansen & Moore 2006; Dehnen & McLaughlin 2005). In detail, the latter suggest the effective linear approximation

$$\beta(r) \approx \beta(0) + \beta'[\gamma(r) - \gamma_a] \tag{5}$$

with $\beta(0) \gtrsim -0.1$ and $\beta' \approx 0.2$, limited to $\beta(r) \lesssim 0.5$. We find (Figure 2) the corresponding $\rho(r)$ to be slightly *flattened* at the center by a weakly negative $\beta(0)$, and considerably *steepened* into the outskirts where $\beta(r)$ grows substantially positive. Specifically, the following simple rules apply: the slope β' in Equation (5) is found to drop out from the derivatives of the Jeans equation (Dehnen & McLaughlin 2005); the upper bound to α now reads $\tilde{\alpha} = 35/27 - 4\beta(0)/27$; γ_a is modified into $\gamma_a = 3\alpha/5 + 6\beta(0)/5$, while γ_0 and γ_b retain their form.

As to the former and minor issue, we include the slowly decreasing run $\alpha(r)$ (e.g., Figure 1) enforced within outskirts developing by slow mass accretion, as the outer scale is stretched out while the body stays put. Clearly, this affects little the inner profile of $\rho(r)$ as Jeans itself (with its inner boundary conditions) works from the inside out, but it tilts *down* $\rho(r)$ appreciably into the outskirts.

In Figure 2, we represent as solid lines the α-profiles *refined* as to include both the declining $\alpha(r)$ and the anisotropies discussed above.

3.2. Testing the α-Profiles and Their Development

Now we turn to testing these refined profiles against the recent, extensive GL observations of the cluster A1689 that join strong and weak lensing to cover scales from 10^{-2} to 2.1 Mpc,

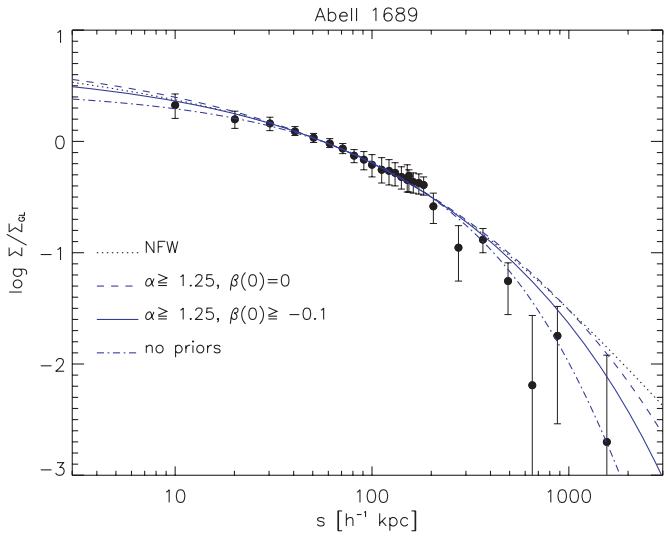

Figure 3. Surface density runs for the cluster A1689. Filled symbols represent the data by Lemze et al. (2008; see also Umetsu & Broadhurst 2008) from joint strong and weak GL observations. Blue lines illustrate fits to the data terms of our α-profiles with no prior (dot-dashed), or with priors: $\alpha \geqslant 1.25$ and $\beta(0) = 0$ (dashed); $\alpha \geqslant 1.25$ and $\beta(0) \geqslant -0.1$ (solid). For comparison, the black dotted line shows the NFW fit. We report in Table 1 the values of the fitting parameters α, $\beta(0)$, and c, and of the corresponding minimum χ^2/dof.

the latter being the virial radius R; see Broadhurst et al. (2005), Halkola et al. (2006), Limousin et al. (2007), and Umetsu & Broadhurst (2008). We focus on the data set presented by the latter authors and refined in Lemze et al. (2008).

These observations concern the surface density, for which our benchmark is constituted by the refined α-profiles integrated over the line of sight at a projected distance s from the center

$$\Sigma(s) = 2 \int_s^R dr \, \frac{r\,\rho(r)}{\sqrt{r^2 - s^2}}. \qquad (6)$$

In Figure 3, we illustrate as blue lines the outcomes of fits to the data in terms of our refined α-profiles; for the anisotropy, we have adopted Equation (5) with $\beta(0)$ as the only effective parameter; see Section 3.1.

The dashed line represents the best fit for isotropic profiles ($\beta = 0$) with the prior $\alpha \geqslant 1.25$ from the two-stage development (see Section 2.1); the solid line refers to the best fit for anisotropic profiles subject to the priors $\alpha \geqslant 1.25$ and $\beta(0) \geqslant -0.1$ from simulations (see Section 3.1); the dot-dashed line refers to the best fit for anisotropic profiles with no prior. For comparison, the black dotted line illustrates the fit with the NFW formula.

In Table 1 we report the corresponding values of the fitting parameters α, $\beta(0)$, and c (with their 68% uncertainty), and of the corresponding minimum χ^2/dof. The physical α-profiles generally provide fits of comparable or better quality than the empirical NFW formula; note that an optimal fit obtains with no priors on α and β, but at the cost of ignoring the information on the former as provided by the two-stage development, and on the latter as provided by the numerical simulations.

We find that *balanced* fits to the surface density in A1689 require $c \approx 10$; lower values would cause wide overshooting of the outer points, while higher ones would allow approaching these (with little impact on χ^2 owing to the large uncertainties) at the cost of overshooting the precise inner points.

A similar balancing has been found by Broadhurst et al. (2008) from fits with the empirical NFW formula, yielding

Table 1
Results of the Fits to the Surface Density of A1689

Reference in Figure 3	α	$\beta(0)$	c	χ^2/dof
NFW	...	...	$12.2^{+3.2}_{-2.7}$	7.94/(26 − 2)
$\alpha \geqslant 1.25$, $\beta(0) = 0$	$1.25^{+0.03}$	0	$10.7^{+3.2}_{-2.5}$	8.78/(26 − 3)
$\alpha \geqslant 1.25$, $\beta(0) \geqslant -0.1$	$1.25^{+0.04}$	$-0.1^{+0.09}$	$11.6^{+2.8}_{-2.4}$	6.55/(26 − 4)
No priors	$1.18^{+0.09}_{-0.13}$	$-0.15^{+0.23}_{-0.21}$	$12.4^{+2.2}_{-2.1}$	4.13/(26 − 4)

Note. For the anisotropy, we have adopted Equation (5), where $\beta(0)$ is the only relevant free parameter, see Section 3.1.

generally high concentrations. These authors suggest that large values of c may be understood in terms of formation redshifts earlier than expected from the standard ΛCDM cosmogony, as quantitatively focused by Sadeh & Rephaeli (2008). From the perspective of our α-profiles, concentrations $c \approx 10$ are strictly related to transition redshifts $z_t \approx 1.5$ based on the state-of-the-art evolution of biased ΛCDM halos, see Equation (2) and Figure 1; on the same ground, we compute their occurrence to be bounded by about 13% in blind sampling.

On the other hand, such early biased halos tend to be favored with GL data. This is because strong GL observations are favored by centrally flat profiles and steep outskirts producing conspicuously large Einstein rings (Broadhurst & Barkana 2008). Meanwhile, weak GL observations require extensive outskirts to affect numerous background galaxies.

For A1689 the latter data with their uncertainties are not yet sharply constraining the fit, but we expect convergence toward the physical profiles as the uncertainties are narrowed down by improved control over the redshift distribution of background galaxies (see Medezinski et al. 2007; Limousin et al. 2007; Umetsu & Broadhurst 2008). On the other hand, more and more clusters are being covered by GL observations, which often find evidence of centrally flat density runs (Bradač et al. 2008; Sand et al. 2008; Richard et al. 2009; Oguri et al. 2009), consistently with our physical α-profiles.

4. DISCUSSION AND CONCLUSIONS

To sum up, the DM halo benchmark we test with GL observations is comprised of a time and a space behavior, that we strictly link in the framework of ΛCDM cosmogony. As to time, we find a *narrow* range of the DM entropy slope α as an outcome of a *two-stage* development comprising an early fast collapse of the body followed by a slow, inside-out growth of the outskirts.

As to space, the physical α-profiles we derive feature density runs $\rho(r)$ intrinsically *flatter* toward the center, and intrinsically *steeper* toward the outskirts as to yield a definite mass, relative to the singular NFW rendition of early N-body data. We find these runs to be stable with, or even *sharpened* by anisotropy.

These physical α-profiles improve at both small and large scales the fits to the GL data, including the extensively probed case of A1689. Here the present analysis requires a halo *biased* toward a main progenitor lineage, with non-standard concentration $c \approx 10$ marking a body collapsed early at $z_t \approx 1.5$ and late extensive outskirts; we find such halos to comprise some 10% of the clusters.

Alternative proposals to relieve the tension of the GL observations with the profiles expected for average clusters include density cores flattened by degenerate pressure (Nakajima & Morikawa 2007), or concentrations enhanced by some 30% owing to sharply prolate triaxialities (see Hennawi et al. 2007;

Oguri & Blandford 2009; Corless et al. 2009) which on the other hand would produce steeper central slopes. The α-profiles and the two-stage development dispense with such contrasting interpretations, providing sharp and consistent shapes linked with early-biased histories. This view clearly invites blind sampling of more clusters in GL.

On the other hand, the X-ray data will provide an *independent* line of evidence concerning profiles and concentrations. This is based on the other major component of clusters, i.e., the intracluster plasma (ICP) which settles to its own equilibrium within the DM potential well, and emits strong X-rays by thermal bremsstrahlung (see Sarazin 1988).

ICP information from spectroscopy (yielding the temperature T) and X-ray brightness (yielding the squared number density n^2) are best combined in the form of the thermodynamic ICP entropy (adiabat) $k(r) \equiv k_B T/n^{2/3}$; this modulates the ICP equilibrium within the DM potential well, and throughout the cluster body follows a power-law run $k(r) \propto r^a$ with $a \lesssim 1.1$.

In fact, Lapi et al. (2005) and Cavaliere et al. (2009) compute the slope a to be expected in the cluster outskirts from accretion of external gas shocked at about the virial R (see also Tozzi & Norman 2001). They find $a \approx 2.37$–$0.71/\Delta\phi(c)$ in terms of the potential drop $v_c^2(R)\,\Delta\phi(c)$ from the turnaround to R; meanwhile, the ICP density follows $n(r) \propto r^{-g}$ with $g \approx 1.42 + 0.47/\Delta\phi(c)$. Values $\Delta\phi \approx 0.56$ are seen to apply for α-profiles with concentration $c \approx 5$, to yield $a \approx 1.1$ and $g \approx 2.2$ as measured in many clusters. But in clusters with extensive outskirts and higher concentrations the outer potential is shallower and $\Delta\phi(c)$ smaller; when $c \approx 10$ one finds $\Delta\phi \approx 0.47$, yielding an intrinsically *flatter* $a \approx 0.85$ (and a steeper $g \approx 2.4$ in the absence of large central energy discharges). This theoretical expectation finds gratifying support in the flat $a \approx 0.8$ observed in A1689 by Lemze et al. (2008).

We note that the α-profiles provide a physical *benchmark* also useful in the context of probing CDM annihilations [$\propto \rho^2(r)$] or decays [$\propto \rho(r)$] through diffuse γ-ray emissions expected from the Galaxy center (e.g., Bertone et al. 2008), and the positron excess recently detected by *PAMELA* (e.g., Adriani et al. 2008). We will investigate the issue elsewhere.

Finally, since a two-stage development also applies to hot DM cosmogonies (though with c decreasing in cosmic time, see Wang & White 2008), we comment upon the case for CDM on the basis of the radial run $\sigma_r^2(r) \propto \rho^{2/3}(r)\,K(r) \propto r^{\alpha - 2\gamma(r)/3}$. We expect that CDM halos will be marked by $\sigma_r^2(r)$ falling down to a few hundreds km s^{-1} into the outskirts, cf., Figure 2 with the dynamical observations by Lemze et al. (2009, their Figure 7). Such a behavior will provide evidence for a truly cold nature of the DM.

This work is partially supported by Agenzia Spaziale Italiana (ASI). We thank T. Broadhurst, R. Fusco-Femiano, E. Medezinski, P. Natoli, and K. Umetsu for informative and useful discussions. We acknowledge the anonymous referee for constructive and helpful comments.

REFERENCES

Adriani, O., et al. 2008, Nature, submitted (arXiv:0810.4995)
Austin, C. G., et al. 2005, ApJ, 634, 756
Bertone, G., et al. 2009, J. Cosmol. Astropart. Phys., JCAP03(2009)009
Bertschinger, E. 1985, ApJS, 58, 39
Binney, J. 1978, MNRAS, 183, 779
Bradač, M., et al. 2008, ApJ, 681, 187
Broadhurst, T., & Barkana, R. 2008, MNRAS, 390, 1647
Broadhurst, T., et al. 2005, ApJ, 619, L143
Broadhurst, T., et al. 2008, ApJ, 685, L9
Cavaliere, A., Lapi, A., & Fusco-Femiano, R. 2009, ApJ, submitted
Cavaliere, A., & Menci, N. 2007, ApJ, 664, 47
Corless, V. L., King, L. J., & Clowe, D. 2009, MNRAS, 393, 1235
Dehnen, W., & McLaughlin, D. E. 2005, MNRAS, 363, 1057
Diemand, J., Kuhlen, M., & Madau, P. 2007, ApJ, 667, 859
Halkola, A., Seitz, S., & Pannella, M. 2006, MNRAS, 372, 1425
Hansen, S. H., & Moore, B. 2006, New Astron., 11, 333
Hennawi, J. F., et al. 2007, ApJ, 654, 714
Hoffman, Y., et al. 2007, ApJ, 671, 1108
Lapi, A., & Cavaliere, A. 2009, ApJ, 692, 174 (LC09)
Lapi, A., Cavaliere, A., & Menci, N. 2005, ApJ, 619, 60
Lemze, D., et al. 2008, MNRAS, 386, 1092
Lemze, D., et al. 2009, ApJ, submitted (arXiv:0810.3129)
Li, Y., et al. 2007, MNRAS, 379, 689
Limousin, M., et al. 2007, ApJ, 668, 643
Medezinski, E., et al. 2007, ApJ, 663, 717
Nakajima, T., & Morikawa, M. 2007, ApJ, 655, 135
Navarro, J. F., Frenk, C. S., & White, S. D. M. 1997, ApJ, 490, 493
Navarro, J. F., et al. 2008, MNRAS, submitted (arXiv:0810.1522)
Oguri, M., & Blandford, R. D. 2009, MNRAS, 392, 930
Oguri, M., et al. 2009, arXiv:0901.4372
Richard, J., et al. 2009, A&A, in press (arXiv:0901.0427)
Sadeh, S., & Rephaeli, Y. 2008, MNRAS, 388, 1759
Salvador-Solé, E., et al. 2007, ApJ, 666, 181
Sand, D. J., et al. 2008, ApJ, 674, 711
Sarazin, C. L. 1988, X-ray Emission from Clusters of Galaxies (Cambridge: Cambridge Univ. Press)
Taylor, J. E., & Navarro, J. F. 2001, ApJ, 563, 483
Tozzi, P., & Norman, C. 2001, ApJ, 546, 63
Umetsu, K., & Broadhurst, T. 2008, ApJ, 684, 177
Vass, I., et al. 2008, MNRAS, submitted (arXiv:0810.0277)
Wang, J., & White, S. D. M. 2008, MNRAS, submitted (arXiv:0809.1322)
Wechsler, R. H., et al. 2006, ApJ, 652, 71
Zhao, D. H., et al. 2003, MNRAS, 339, 12